

# Frequency-Fixed Beam-Scanning Leaky-Wave Antenna Using Electronically Controllable Corrugated Microstrip Line

Meng Wang, Hui Feng Ma<sup>ID</sup>, Hao Chi Zhang<sup>ID</sup>, *Student Member, IEEE*, Wen Xuan Tang<sup>ID</sup>, *Member, IEEE*, Xuan Ru Zhang<sup>ID</sup>, and Tie Jun Cui<sup>ID</sup>, *Fellow, IEEE*

**Abstract**—An electronically controllable microstrip leaky-wave antenna (LWA) to steer the radiations at a fixed frequency is presented. The proposed LWA is composed of a corrugated microstrip line loaded by the varactor diodes with triangular-modulated surface impedance. Due to the periodical modulation of the surface impedance, the guided waves can be converted into the leaky-wave radiations efficiently with frequency-scanning property. Furthermore, the surface impedance of the LWA can be reconfigured by changing the capacitance of the varactor diode through dc bias voltage, which will make the radiation beam steer in a large angle range accordingly at a fixed frequency. Both numerical simulations and experimental results show that the radiation beams can be controlled for continuously steering at each frequency from 5.5 to 5.8 GHz by changing the dc bias voltage from 0 to 20 V, in which the scanning angle can reach as high as 45°.

**Index Terms**—Electronically controlled beam scanning, leaky-wave antennas (LWAs), surface impedance modulation.

## I. INTRODUCTION

LEAKY-WAVE antennas (LWAs), which are kinds of travelling-wave antennas, have attracted much attention due to their unique advantages, such as low profile, high gain, and low cost. The concept of leaky wave was first proposed by Hansen [1] through slit slots on a waveguide. Thereafter, many LWAs based on different wave-guiding structures have been proposed, including microstrip line [2], coaxial cable [3], substrate integrated waveguide [4], [5], composite right/left-handed transmission line (CRLH TL) [5], [6], and spoof surface plasmon polariton waveguide [7]–[9]. Generally, LWAs can be divided into two categories according to their working principle. One is the quasi-uniform LWAs, whose periodic corrugations have a period

Manuscript received September 18, 2017; revised April 17, 2018; accepted May 25, 2018. Date of publication June 13, 2018; date of current version August 31, 2018. This work was supported in part by the National Science Foundation of China under Grant 61522106, Grant 61571117, Grant 61501117, Grant 61501112, Grant 61631007, and Grant 61701108, in part by the National Instrumentation Program under Grant 2013YQ200647, in part by the 111 Project under Grant 111-2-05, and in part by the Natural Science Foundation of Jiangsu Province under Grant BK20150020. (*Meng Wang and Hui Feng Ma contributed equally to this work.*) (*Corresponding author: Hui Feng Ma.*)

The authors are with the State Key Laboratory of Millimeter Waves, Southeast University, Nanjing 210096, China, and also with the Synergetic Innovation Center of Wireless Communication Technology, Nanjing 210096, China (e-mail: hfma@seu.edu.cn; tj cui@seu.edu.cn).

Color versions of one or more of the figures in this paper are available online at <http://ieeexplore.ieee.org>.

Digital Object Identifier 10.1109/TAP.2018.2845452

lower than half-wavelength, and these kinds of LWAs usually have the limitation of frequency scanning in the front quadrant [4]. The other is the periodic-modulated LWAs, which have a period in the order of half-wavelength, and the  $n = -1$  space harmonic is designed to make a radiation which allows for backward-to-forward radiation [10], [11]. However, the periodically modulated LWAs usually suffer from the open-stopband (OSB) at broadside [12]. The LWAs based on the CRLH TL also allow for backward-to-forward scanning from the  $n = 0$  space harmonic using metamaterial unit cells without OSB effect [13].

The real-time manipulation of leaky-wave steering at a fixed frequency has always been a hot topic in the area of LWAs [14]–[18]. Based on the type of quasi-uniform LWAs, a 1-D Fabry–Perot (FP) LWA has been reported to achieve electronic scanning from 9° to 30° at 5.6 GHz in the front quadrant by using tunable high impedance surface [14], and then the scanning angle was enlarged to 29° at 6 GHz by independently controlling the connection of loaded capacitor in each unit cell of a half-width microstrip LWA [15] at the price of much more complicated bias circuit. In order to obtain the continuous beam scanning from backward-to-forward direction, another FP LWA has been presented by using a central feed to obtain a continuous electronic scanning from –25° to 25° at 5.5 GHz [16]. It was also reported that 17.5° beam scanning could be achieved from backward-to-forward direction at a fixed frequency by changing the bias voltage of loaded-varactor in CRLH structure [17]. Based on periodically modulated LWA, an electronically tunable LWA was proposed to realize fixed-frequency beam scanning in the forward quadrant based on sinusoidal modulations of reactance surface [18]. However, it is difficult to place varactor diodes and add dc bias in practice, and hence only simulation results were presented in [18].

In this paper, we propose an electronically controllable LWA using corrugated microstrip line (CML) with triangular modulation of surface impedance to control the leaky-wave steering in real time at a fixed frequency. The LWA consists of a corrugated metallic strip decorated with periodically modulated subwavelength grooves and a metal ground spaced by a substrate dielectric. Due to the periodic modulation of the surface impedance by changing the groove depth, one can efficiently modulate and convert the guided waves to the leaky-wave radiations with frequency-scanning properties,

and the radiation direction is dependent on the modulation of surface impedance [7], [19], [20]. However, under the passive condition, the radiation direction of the leaky wave cannot be controlled at a fixed frequency once the design is completed. In order to realize fixed-frequency beam scanning, varactor diodes are added in the LWA to provide reconfigurable surface impedance since their capacitances can be easily changed through the bias voltage. Then, the radiation direction of the leaky wave can steer in a programmable way at a fixed frequency. Finally, we design, fabricate, and measure the electronically controllable LWA, in which the measured results have good agreements with numerical simulations. We show that the scanning range of leaky-wave radiations can reach 45° at every frequency from 5.5 to 5.8 GHz. Moreover, the OSB effect has been discussed and solved by adding a matching stub (MS) in each period of the LWA, and the simulation results show that the radiation efficiencies are improved significantly at broadside radiation.

## II. THEORIES AND SIMULATIONS

According to knowledge of the LWA, the guided waves can be converted to leaky-wave radiations if the surface impedance of the transmission line (TL) is modulated sinusoidally [7], [19], [20]

$$Z_s(x) = jX_s \left[ 1 + M \cos \left( \frac{2\pi x}{P} \right) \right] \quad (1)$$

in which  $X_s$  is the average surface reactance,  $M$  is the modulation factor, and  $P$  is the modulation period. The first harmonic, which is the first radiating harmonic, is usually designed to generate the leaky-wave radiation, whose radiation angle can be calculated as

$$\theta_{-1} = \arcsin \left( \sqrt{1 + X'^2} - \frac{2\pi}{k_0 p} \right) \quad (2)$$

in which  $X' = X_s/\eta_0$  is the average surface reactance,  $\eta_0$  is the free-space wave impedance, and  $k_0$  is the free-space wavenumber.

In this designing, the LWA is realized by choosing a CML with triangular-modulated surface impedance for simplifying the model of the varactor diodes loaded CML, whose surface impedance is written as

$$Z_s(x) = \begin{cases} jX_s \left( 1 + \frac{2M}{P}x - \frac{M}{2} \right) & \text{if } 0 \leq x \leq \frac{P}{2} \\ jX_s \left( 1 - \frac{2M}{P}x + \frac{3M}{2} \right) & \text{if } \frac{P}{2} \leq x \leq P \end{cases} \quad (3)$$

where  $X_s$ ,  $M$ , and  $P$  are the same as those in (1). We remark that the radiation angle of the beam based on the triangular modulation also can be calculated by using (2) [21].

The schematic of the LWA with triangularly modulated surface impedance is demonstrated in Fig. 1, which is composed of a corrugated metallic strip and a metal ground spaced by a dielectric substrate of F4BK350 with relative permittivity 3.5 and loss tangent 0.001. The thicknesses of dielectric substrate and covering copper are 3 and 0.018 mm, respectively, and the total length of the LWA is 330.8 mm. The dimensions shown in Fig. 1 are  $d = 4.708$  mm,  $a = 0.6d$ ,

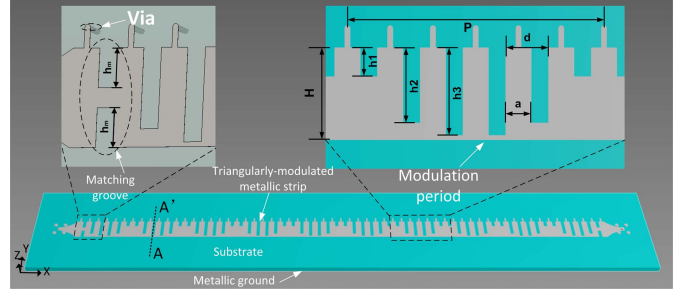


Fig. 1. Schematic of triangularly modulated LWA using CML.

$H = 10$  mm,  $P = 6d = 28.248$  mm, and the groove depths are  $h_1$ ,  $h_2$ , and  $h_3$ , respectively. At each terminal of the LWA, a notch groove with dimension of  $4 \times 1.8832$  mm<sup>2</sup> is used for impedance matching between the terminal and the corrugated metallic strip.

The dispersion curves of the unit cell with different groove depths are simulated by using full-wave commercial software, CST Microwave Studio, and shown in Fig. 2(a) with solid lines. Then, the surface impedance of the LWA can be calculated as

$$Z_s = j\eta_0 \sqrt{(k_x/k_0)^2 - 1} \quad (4)$$

in which  $k_x$  is the wavenumber of the LWA along the propagating direction. The finally calculated surface impedance ( $Z_s$ ) versus the wavenumber ( $k_x$ ) is demonstrated as the dashed lines shown in Fig. 2(a).

The radiation angle of the leaky-wave beam is related to both the modulating period ( $P$ ) and the average surface reactance ( $X_s$ ) according to (2), while the modulating period of  $P = 28.248$  mm is always fixed in this design, so the radiation angle of the beam only depends on  $X_s$ . For example, if we design a radiation beam directing to  $\theta_{-1} = 16^\circ$  at 5.6 GHz, then  $X_s = 726.3$  Ω can be obtained from (2). The surface impedance ranges from the minimum value of 435.7 Ω to the maximum value of 985.6 Ω as the groove depth changes from 1 to 9.5 mm, as shown in Fig. 2(a). Hence, we choose  $M = 0.37$  to make the range of the surface impedances as large as possible and consequently obtain highly efficient radiation. Then, the groove depths of the triangularly modulated LWA can be finally determined according to the relationship between  $Z_s$  and  $h$  at 5.6 GHz, as is shown by the red dashed lines in Fig. 2(a). The finally calculated groove depths are  $h_1 = 3.137$  mm,  $h_2 = 8.164$  mm, and  $h_3 = 9.51$  mm. Fig. 2(b) demonstrates the simulated power-density distributions in the plane of  $y = 0$  and the cross section of AA' (inset at the upper left corner) at 5.6 GHz, which show that the EM energy is mainly confined on the upper surface of the corrugated metallic strip and radiates to the direction of  $\theta = 15.5^\circ$ . Fig. 2(c) shows the simulated 3-D far-field radiation pattern at 5.6 GHz with the main beam directing to  $15.5^\circ$ , which agrees well with the theoretical calculation. The radiation angles of the beam at other frequencies can also be calculated from (2), whose simulated far-field radiation patterns are shown in Fig. 2(d), which are consistent very well with the calculation results given in Table I. We remark that

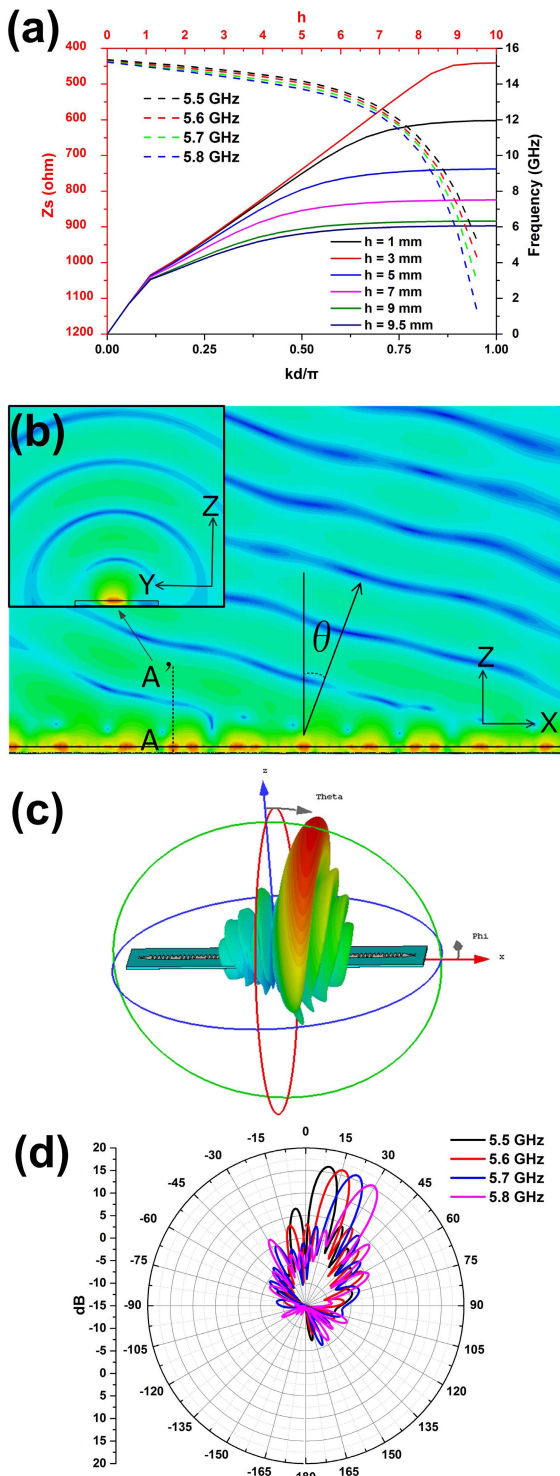


Fig. 2. Dispersion curves and the simulation results of the LWA. (a) Dispersion curves and the surface impedances of the unit. (b) Power-density distributions in the plane of  $y = 0$  and the cross section of AA' (inset at the upper left corner) at 5.6 GHz. (c) 3-D far-field radiation patterns at 5.6 GHz. (d) 2-D far-field radiation patterns when frequency changes from 5.5 to 5.8 GHz.

the radiations are linearly polarized transverse electromagnetic waves with electric-field vector paralleling to the  $xoz$  plane.

However, from above discussions, the radiation beam can steer as frequency changes but becomes nonsteerable at a

TABLE I  
CALCULATED AND SIMULATED RADIATION ANGLES OF THE BEAM AT DIFFERENT FREQUENCIES

Freq./GHz	5.5	5.6	5.7	5.8
Cal.	10.2°	16.0°	23.2°	32.2°
Sim.	10.0°	15.5°	22.3°	29.5°

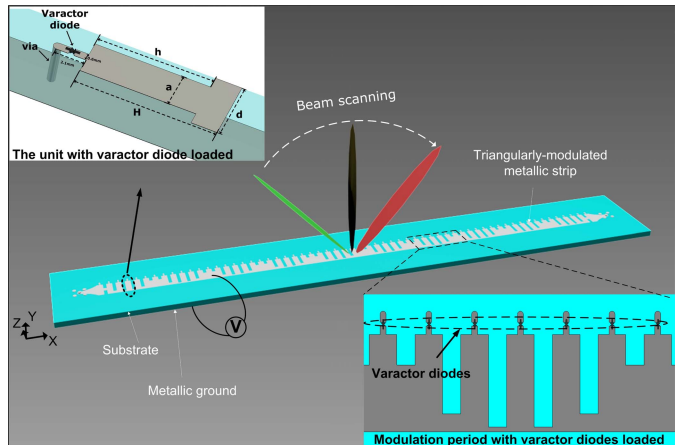


Fig. 3. Schematic of the LWA loaded with varactor diodes.

fixed frequency. In order to realize fixed-frequency beam scanning, we add varactor diodes to the design of LWA, which are connected between the grooves of the corrugated metallic strip and the metal ground through via holes, as shown in Fig. 3. When the bias voltage applied between the corrugated metallic strip and the metal ground, the capacitance value of the varactor diodes can be tuned accordingly. In this way, the surface impedance of the LWA can be reconfigured at a fixed frequency, and then the radiation beam can be steered correspondingly.

In order to predict accurate radiation direction of the beam with different capacitance values of the loaded-varactor diode, we should first obtain the relationship between the capacitance and the surface impedance  $Z_s$  from simulations. However, the lumped capacitor cannot be added in the Eigenmode Solver of CST Microwave Studio. To solve the problem, we use an equivalent model of parallel-plate capacitor to replace the lumped capacitors in the Eigenmode simulations. The equivalent model is a sandwiched structure composed of two metallic slabs spaced by a dielectric block, as shown in Fig. 4(a). Hence, the initial permittivity of the dielectric block can be simply calculated as  $\epsilon_c = \epsilon_0 \cdot L_2 \cdot C / (W_1 \cdot W_2)$ , in which  $C$  is the capacitance of the lumped capacitor, and  $W_1$ ,  $W_2$ , and  $L_2$  are the geometrical parameters as shown in Fig. 4(a). However, this formula is only suitable for an ideal model of parallel-plate capacitor, and hence  $\epsilon_c$  must be optimized to make sure the model shown in Fig. 4(a) is exactly equivalent to the lumped capacitor with the capacitance  $C$ . For instance, if the lumped capacitor with capacitance of  $C$  is loaded in the LWA, then we obtain the accurate radiation angle  $\theta_1$  of the beams directly from the full-wave simulation by the loaded lumped capacitor based on the model shown in Fig. 3. On the other hand, the lumped capacitor with the capacitance  $C$  can

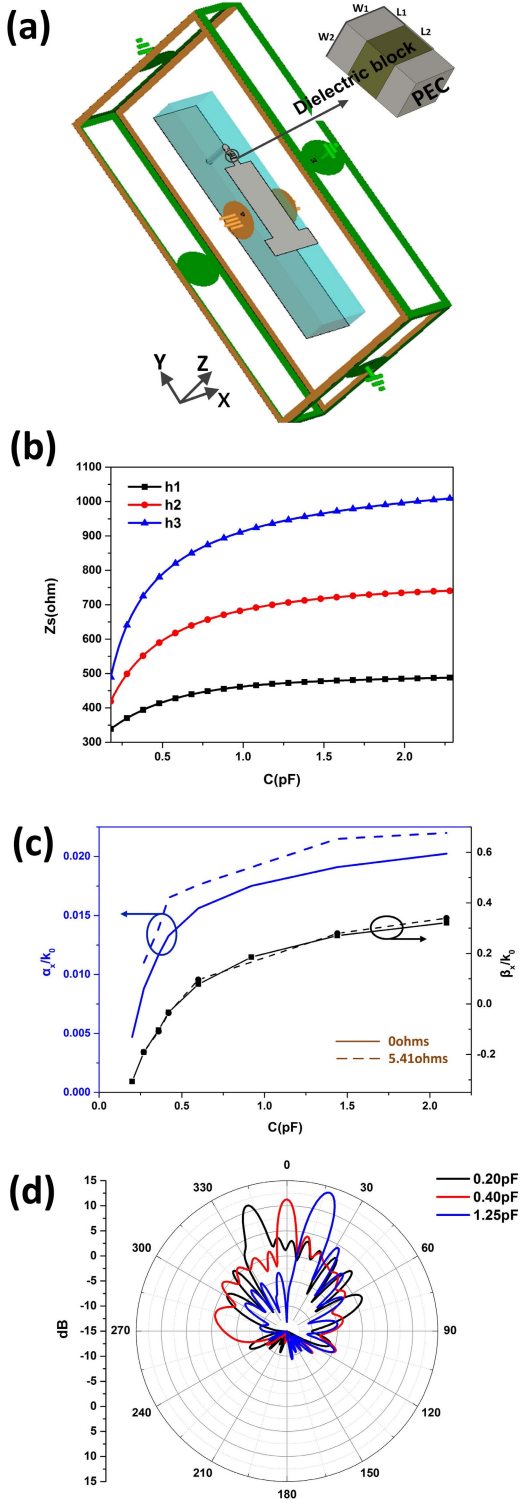


Fig. 4. Equivalent model of the capacitor-loaded unit cell and the related calculation and simulation results at 5.8 GHz. (a) Equivalent model of the unit cell in Eigenmode simulation environment. (b) Curves of surface impedance ( $Z_s$ ) with respect to capacitance value for groove depth of  $h_1 = 3.137$  mm,  $h_2 = 8.164$  mm, and  $h_3 = 9.51$  mm, respectively. (c) Normalized attenuation constant  $\alpha_x/k_0$  and phase constant  $\beta_x/k_0$ . (d) Full-wave simulated 2-D far-field radiation patterns with loaded capacitances of 0.20, 0.40, and 1.25 pF, respectively.

be equivalent to the abovementioned parallel-plate capacitor with an initial permittivity  $\epsilon_c$ , so the propagating constants  $k_x$  for different groove depths can be obtained by using

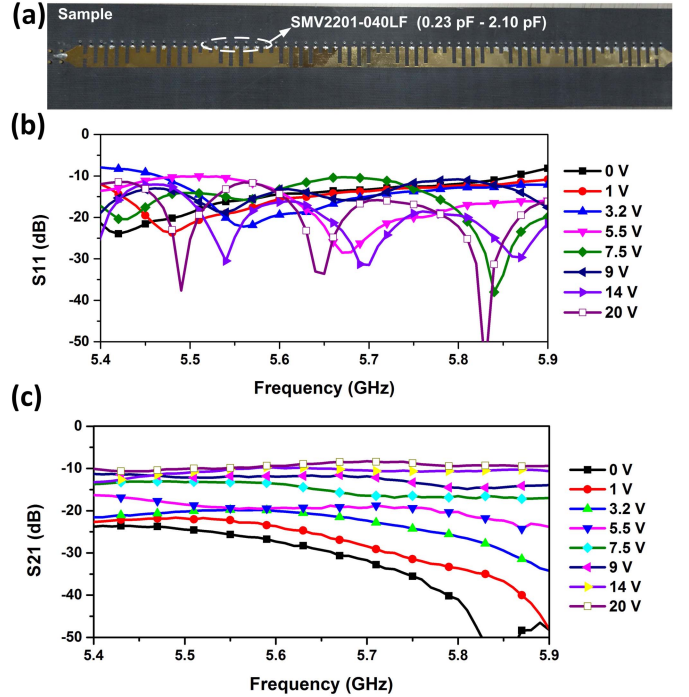


Fig. 5. Experimental sample of LWA and the measured S-parameters with different bias voltages loaded. (a) Experimental sample. (b) Measured reflection coefficients ( $S_{11}$ ). (c) Measured transmission coefficients ( $S_{21}$ ).

the eigenmode simulation as shown in Fig. 4(a), and then a radiation angle ( $\theta_2$ ) of the beam can be calculated theoretically from (2)–(4). To make sure the theoretical calculations are consistent with the full-wave simulations, the permittivity  $\epsilon_c$  of the equivalent model must be optimized to make  $\theta_2 = \theta_1$ . Then, the surface impedances  $Z_s$  of the unit cells can be calculated from (4) by using the optimized equivalent model. The final  $Z_s$ - $C$  curves of the unit cells with different tooth depths ( $h_1 = 3.137$  mm,  $h_2 = 8.164$  mm, and  $h_3 = 9.51$  mm) at 5.8 GHz are demonstrated in Fig. 4(b) by sampling capacitances of  $C = 0.23, 0.27, 0.36, 0.42, 0.60, 0.92, 1.44$ , and  $2.10$  pF.

Furthermore, based on the  $Z_s$ - $C$  curve, the leaky-wave rate  $\alpha$  and the phase constant  $\beta$  can be theoretically calculated [19] as shown in Fig. 4(c) with the solid lines. The normalized attenuation constant  $\alpha_x/k_0$ , and it increases gradually from 0.0035 to 0.021 as the capacitance changes from  $C = 0.2$  pF to  $C = 2.1$  pF at 5.8 GHz, which implies that the higher radiation efficiency and gain will be achieved as the capacitance increases. The normalized  $\beta_x/k_0$  increases from  $-0.3$  to  $0.32$  as capacitance changes from  $C = 0.2$  pF to  $C = 2.1$  pF. Since the radiation angle of leaky waves can be approximately obtained by  $\sin\theta \approx \beta_x/k_0$ , the main beam of the leaky wave can be qualitatively predicted to scan from backward quadrant to forward quadrant continuously at 5.8 GHz by changing the capacitance of varactor diodes from 0.2 to 2.1 pF. It should be noted that the above  $\alpha_x$  and  $\beta_x$  are calculated based on the lossless varactor diodes, assuming that the parasitic resistance ( $R$ ) is  $0 \Omega$ . However, the parasitic resistance of the varactor diode is unavoidable in practical applications, so we further calculate the  $\alpha_x/k_0$  and  $\beta_x/k_0$  with  $R = 5.41 \Omega$  as

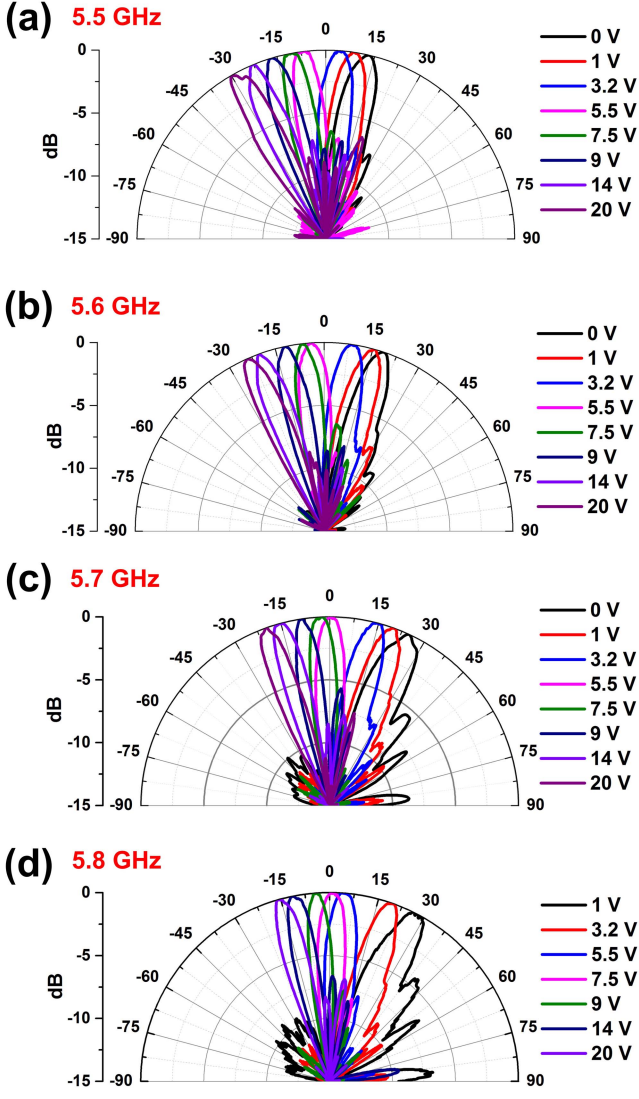


Fig. 6. Measured far-field radiation patterns with different bias voltages loaded. (a) 5.5 GHz. (b) 5.6 GHz. (c) 5.7 GHz. (d) 5.8 GHz.

shown in Fig. 4(c) with the dashed lines [22]. We remark that  $R = 5.41 \Omega$  is consistent with parasitic resistance of varactor diode (SMV2201-40LF) used in the following experiment. The results show that the parasitic resistance has little influence on the  $\beta_x/k_0$  but the  $\alpha_x/k_0$  is increased, which means the direction of the radiation beam is not influenced, but the radiation power is partially consumed by the ohmic dissipation.

According to the  $Z_s-C$  curves shown in Fig. 4(b), the radiation angle of the beam radiated by the LWA loaded with any capacitance can be predicted accurately by using (2)–(4). For example, when  $C = 0.2 \text{ pF}$ , which is not included in above capacitance sampling values, the calculated radiation angle is  $-17.4^\circ$  at 5.8 GHz, which is very close to the full-wave simulated radiation angle of  $-16.2^\circ$  [see the black solid line shown in Fig. 4(d)]. When the capacitance is increased to 0.4 and  $1.25 \text{ pF}$ , the radiation beam will steer and direct to  $0^\circ / -1.1^\circ$  (simulation/calculation) and  $18.9^\circ / 17.3^\circ$ , respectively, as demonstrated in Fig. 4(d), showing a good agreement between the calculation and the simulation. However, because

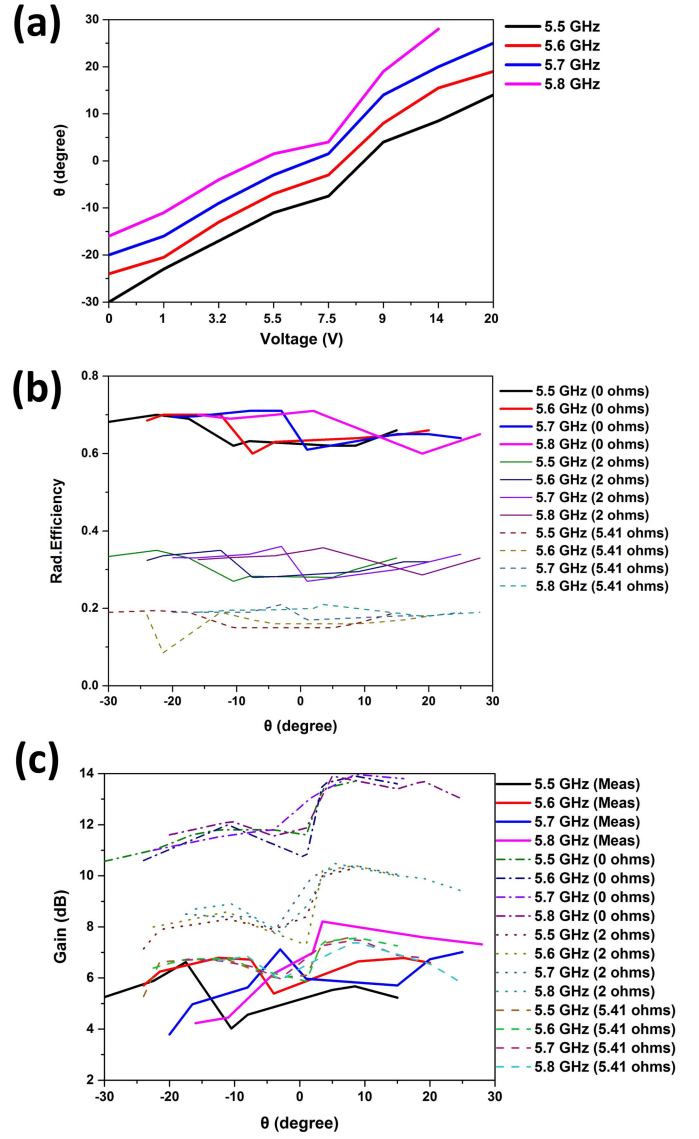


Fig. 7. Simulation and measurement results at different frequencies. (a) Measured scanning angle versus control bias voltage. (b) Simulated radiation efficiency versus pointing angle for different parasitic resistances. (c) Simulated and measured gain versus pointing angle for different parasitic resistances.

the equivalent model is not wideband, the radiation angles of the beams must be recalculated by using the above steps when the frequency changes. In theory, the largest scanning range of the beam can reach about  $55^\circ$  at 5.8 GHz if the loaded capacitance is varied from 0.15 to 10 pF.

### III. FABRICATION AND EXPERIMENT

We design and fabricate the electronically controllable LWA, as shown in Fig. 5(a), which is composed of a metallic corrugated strip and a metal ground spaced by a dielectric substrate with permittivity 3.5 and loss tangent 0.001. The type of loaded-varactor diode we choose is SMV2201-040LF, whose capacitance values are relative to the voltages, as shown in Table II. We remark that the parasitic resistance of the varactor diode SMV2201-040LF is  $5.41 \Omega$  and a BIAS-TEE

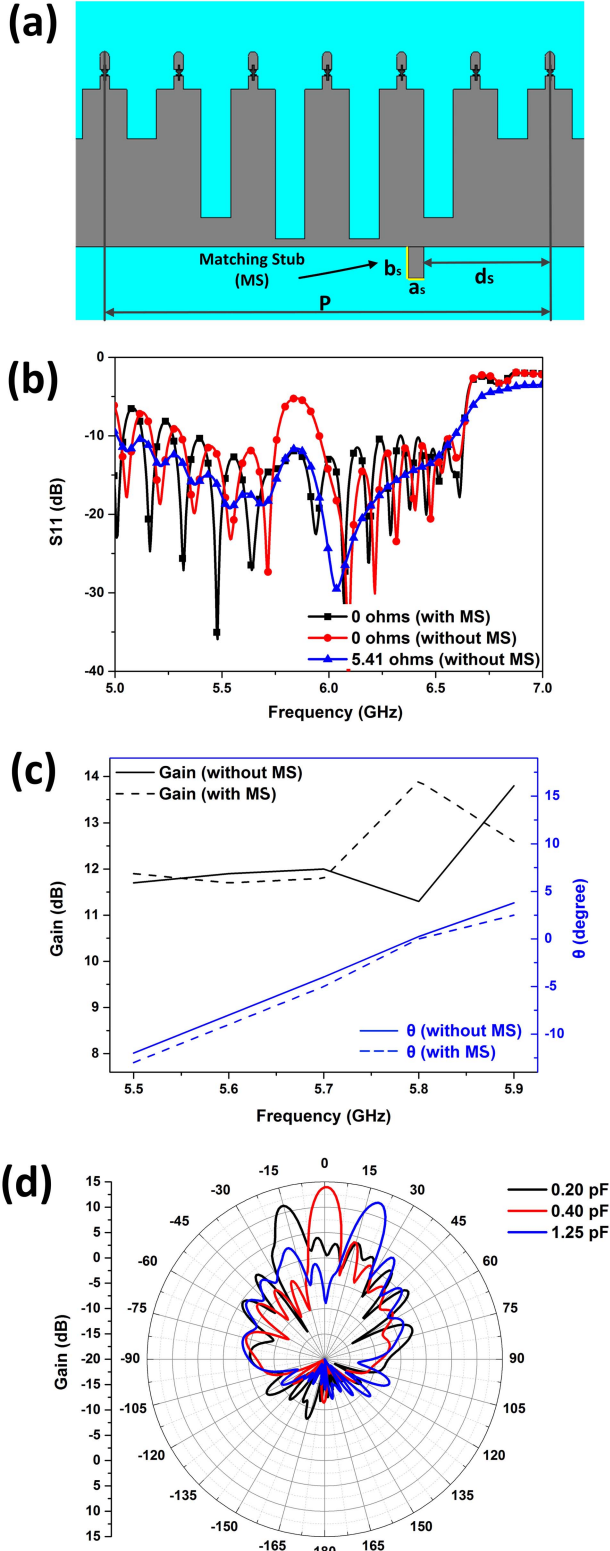


Fig. 8. Model of LWA loaded with a matching stub in each period and the simulation results. (a) Period of LWA loaded with a matching stub. (b)  $S_{11}$ . (c) Gain and scanning angle. (d) Far-field radiation patterns at 5.8 GHz with loaded capacitances of 0.20, 0.40, and 1.25 pF, respectively.

has been used as the bias network to load voltage and radio frequency signals to the LWA. The measured S-parameters of the LWA are presented in Fig. 5(b) and (c), showing that

TABLE II  
RELATIONSHIP BETWEEN THE CAPACITANCES AND BIAS VOLTAGES FOR VARACTOR DIODE OF SMV2201-040LF

Vol. (V)	0	1	3.2	5.5	7.5	9	14	20
Cap. (pF)	2.10	1.44	0.92	0.60	0.42	0.36	0.27	0.23

TABLE III  
RADIATION ANGLES OF THE BEAM AT 5.8 GHz ACHIEVED FROM CALCULATIONS, SIMULATIONS, AND EXPERIMENT, RESPECTIVELY

	0.23 pF (20 V)	0.27 pF (14 V)	0.36 pF (9 V)	0.42 pF (7.5 V)	0.6 pF (5.5 V)	0.94 pF (3.2 V)	1.44 pF (1 V)
Cal	-14°	-11°	-3°	0°	6°	14°	19°
Sim	-14°	-10°	-3°	1°	6°	14°	20°
Exp	-16°	-11°	-3°	1°	5°	19°	27°

both reflection ( $S_{11}$ ) and transmission ( $S_{21}$ ) coefficients are lower than  $-10$  dB as the bias voltage changes from 0 to 20 V. Then, we measure the far-field radiation patterns of the beam controlled by the bias voltage at different frequencies, as demonstrated in Fig. 6. We note that the large scanning angle of the beam reaches  $43^\circ$ ,  $44^\circ$ ,  $47^\circ$ , and  $45^\circ$  at 5.5, 5.6, 5.7, and 5.8 GHz, respectively, by changing the bias voltage from 0 to 20 V. We compare the measured results with the calculated and simulated ones at 5.8 GHz, as listed in Table III, which have good agreements with each other.

Fig. 7(a) shows the measured radiation angle of the beam versus bias voltage at different frequencies, which show that the beams can be controlled to steer from backward quadrant to forward quadrant continuously. It should be noted that the increase of the parasitic resistance of the varactor diodes in the experiment has little influence on the radiation angle as shown in Fig. 7(a), but brings in a great influence on the radiation efficiency and gain, as shown in Fig. 7(b) and (c), which have a good agreement with the calculated attenuation constant  $\alpha$  and the phase constant  $\beta$  demonstrated in Fig. 4(c). When the parasitic resistance increases from 0 to  $5.41 \Omega$ , the radiation efficiency declines from about 68% to 20% [Fig. 7(b)] and the gain decreases from about 12 to 6 dB [Fig. 7(c)]. We remark that the measured gains are consistent very well with the simulated ones if the  $5.41 \Omega$  parasitic resistance is added into the varactor diodes. From above discussion, we can conclude that the low radiation efficiency and gain of the designed LWA in the experiment are mainly caused by the large parasitic resistance of the varactor diode SMV2201-040LF. As a result, low-loss varactor diode can be applied to replace the SMV2201-040LF diodes in this design to effectively improve the radiation efficiency and gain.

#### IV. DISCUSSION OF OPEN-STOPBAND EFFECT

The periodically modulated LWAs usually suffer from an OSB at broadside radiation with low radiation efficiency [12], [23]–[25]. In order to investigate the OSB effect of the LWA proposed in this paper, we first analyze the S-parameters of the waveguide, as shown in Fig. 8(b). We assume that the loaded capacitance is  $C = 0.4$  pF, when the parasitic resistance is  $5.41 \Omega$ , which is the same

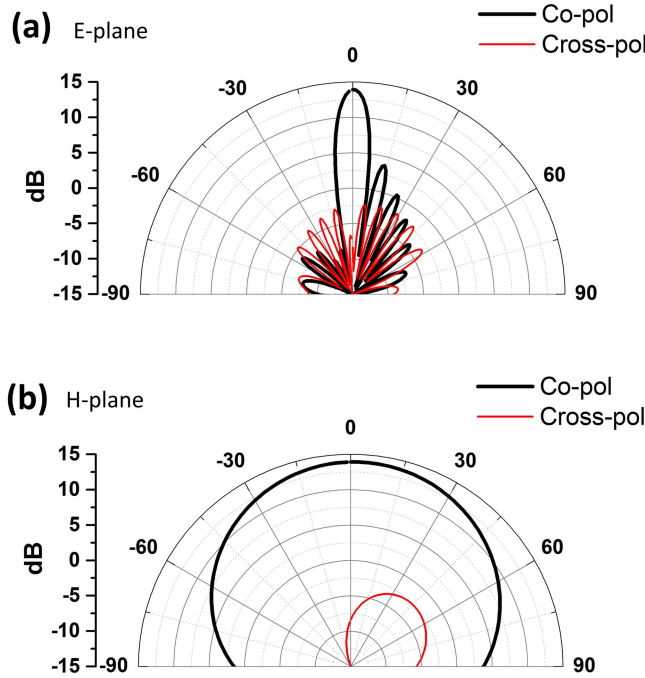


Fig. 9. Simulated far-field radiation patterns of the LWA at 5.8 GHz with loaded capacitance of 0.40 pF. (a) E-plane. (b) H-plane.

as that of the varactor diode SMV2201-040LF used in the experiment, the OSB effect still can be observed from the  $S_{11}$  parameter, as shown by the solid blue line in Fig. 8(b). However, the level of  $S_{11}$  is lower than  $-10$  dB in the whole frequency range, which is mainly due to the large loss of the parasitic resistance introduced by the varactor diode SMV2201-040LF. So, the radiation efficiency is decreased greatly within the whole band and the OSB effect cannot be clearly observed from the radiation efficiency and gain as demonstrated in Section III. When the parasitic resistance is decreased to 0 (lossless), the OSB effect can be observed obviously from the sudden rise of the reflection coefficient ( $S_{11}$ ) at broadside radiation around 5.8 GHz, as shown by the red solid line in Fig. 8(b), and the gain has a sudden decrease as shown by the black solid line in Fig. 8(c).

In order to improve the radiation efficiency at broadside radiation, we add a MS in every period of the original LWA to reduce the reflection [24] as shown in Fig. 8(a), in which the MS is located at  $d_s = 14.7$  mm away from the end of each period with the size of  $a_s \times b_s = 1$  mm  $\times$  2 mm. The reflection coefficients of the lossless LWA with MS can be decreased greatly at broadside radiation (5.8 GHz) as shown by the red solid line in Fig. 8(b), and the gain can be increased from 11.6 to 13.7 dB at 5.8 GHz compared to the original LWA without MS as shown in Fig. 8(c), while the radiation angles are slightly influenced as shown by the blue lines in Fig. 8(c). Fig. 8(d) shows that the radiation beam steers from backward quadrant ( $-15^\circ$ ) to forward quadrant ( $17^\circ$ ), passing through broadside ( $0^\circ$ ), when the capacitance of the loaded-varactor diode changes from 0.2 to 1.25 pF at 5.8 GHz,

in which the gain is increased obviously at broadside radiation compared to that shown in Fig. 4(d). Hence, the OSB can be suppressed effectively by adding the MS into the LWA, and the highly efficient backward-to-forward continuous scanning can be achieved by the designed electronically controllable LWA if varactor diodes with small or near-zero parasitic resistance can be found to replace the high-loss varactor diodes SMV2201-040LF in the experiment.

Furthermore, the simulated far-field radiation patterns of the LWA with MS at broadside are plotted in Fig. 9, which show a narrow beam and a wide beam in E-plane ( $xoz$  plane) and H-plane ( $yoz$  plane) with low cross-polarization level, respectively.

## V. CONCLUSION

We proposed a kind of electronically controllable LWA, which can control the radiation direction of the leaky wave in real time with a wide scanning angle at a fixed frequency by changing the bias voltages of varactor diodes. The surface impedance of the proposed LWA is modulated triangularly by designing the groove depths of the corrugated metallic strip. Infinite space harmonics are generated by the LWA, in which the one-order space harmonic is chosen to obtain a single-beam radiation. However, the radiation direction of the leaky-wave beam only steers as the frequency changes, which cannot continuously scan at a fixed frequency. In order to realize continuous beam steering at a fixed frequency, we added the varactor diodes in designing the LWA to reconfigure its surface impedance by changing the dc bias voltage, so that the beam can steer continuously as the bias voltage increases or decreases gradually. Finally, we designed, fabricated, and measured the electronically controllable LWA, in which the measured results have good agreements with the calculations and simulations, showing that the radiation beam can scan continuously in a wide range (about  $45^\circ$ ) by changing the bias voltage from 0 to 20 V at each frequency from 5.5 to 5.8 GHz. We also provided a solution to improve the OSB effect at broadside radiation. However, due to the ohmic losses of the varactor resistance, the designed LWA suffers from low radiation efficiency (20%) and thus low-loss varactor diodes are needed for more efficient designs of this electronically controlled LWA.

## REFERENCES

- [1] W. W. Hansen, "Radiating electromagnetic wave guide," U.S. Patent 2402622 A, Jun. 25, 1946.
- [2] A. A. Oliner, "Leakage from higher modes on microstrip line with application to antennas," *Radio Sci.*, vol. 22, no. 6, pp. 907–912, Nov. 1987.
- [3] J. H. Wang and K. K. Mei, "Theory and analysis of leaky coaxial cables with periodic slots," *IEEE Trans. Antennas Propag.*, vol. 49, no. 12, pp. 1723–1732, Dec. 2001.
- [4] J. Liu, D. R. Jackson, and Y. Long, "Substrate integrated waveguide (SIW) leaky-wave antenna with transverse slots," *IEEE Trans. Antennas Propag.*, vol. 60, no. 1, pp. 20–29, Jan. 2012.
- [5] Y. D. Dong and T. Itoh, "Composite right/left-handed substrate integrated waveguide and half mode substrate integrated waveguide leaky-wave structures," *IEEE Trans. Antennas Propag.*, vol. 59, no. 3, pp. 767–775, Mar. 2011.
- [6] F. P. Casares-Miranda, C. Camacho-Penalosa, and C. Caloz, "High-gain active composite right/left-handed leaky-wave antenna," *IEEE Trans. Antennas Propag.*, vol. 54, no. 8, pp. 2292–2300, Aug. 2006.

- [7] G. S. Kong, H. F. Ma, B. G. Cai, and T. J. Cui, "Continuous leaky-wave scanning using periodically modulated spoof plasmonic waveguide," *Sci. Rep.*, vol. 6, Jul. 2016, Art. no. 29600.
- [8] A. Kianinejad, Z. N. Chen, and C.-W. Qiu, "Spoof surface plasmon-based leaky wave antennas," presented at the Asia-Pacific Microw. Conf. (APMC), New Delhi, India, Dec. 2016, pp. 1–3.
- [9] A. Kianinejad, Z. N. Chen, and C.-W. Qiu, "A single-layered spoof-plasmon-mode leaky wave antenna with consistent gain," *IEEE Trans. Antennas Propag.*, vol. 65, no. 2, pp. 681–687, Feb. 2017.
- [10] D. K. Karmokar and K. P. Esselle, "Periodic U-slot-loaded dual-band half-width microstrip leaky-wave antennas for forward and backward beam scanning," *IEEE Trans. Antennas Propag.*, vol. 63, no. 12, pp. 5372–5381, Dec. 2015.
- [11] A. M. Patel and A. Grbic, "A printed leaky-wave antenna based on a sinusoidally-modulated reactance surface," *IEEE Trans. Antennas Propag.*, vol. 59, no. 6, pp. 2087–2096, Jun. 2011.
- [12] P. Burghignoli, G. Lovat, and D. R. Jackson, "Analysis and optimization of leaky-wave radiation at broadside from a class of 1-D periodic structures," *IEEE Trans. Antennas Propag.*, vol. 54, no. 9, pp. 2593–2604, Sep. 2006.
- [13] A. Lai, T. Itoh, and C. Caloz, "Composite right/left-handed transmission line metamaterials," *IEEE Microw. Mag.*, vol. 5, no. 3, pp. 34–50, Sep. 2004.
- [14] R. Guzman-Quiros, J. L. Gomez-Tornero, A. R. Weily, and Y. J. Guo, "Electronically steerable 1-D Fabry-Pérot leaky-wave antenna employing a tunable high impedance surface," *IEEE Trans. Antennas Propag.*, vol. 60, no. 11, pp. 5046–5055, Nov. 2012.
- [15] D. K. Karmokar, K. P. Esselle, and S. G. Hay, "Fixed-frequency beam steering of microstrip leaky-wave antennas using binary switches," *IEEE Trans. Antennas Propag.*, vol. 64, no. 6, pp. 2146–2154, Jun. 2016.
- [16] R. Guzman-Quiros, J. L. Gomez-Tornero, A. R. Weily, and Y. J. Guo, "Electronic full-space scanning with 1-D Fabry-Pérot LWA using electromagnetic band-gap," *IEEE Antennas Wireless Propag. Lett.*, vol. 11, pp. 1426–1429, Nov. 2012.
- [17] S. Lim, C. Caloz, and T. Itoh, "Electronically scanned composite right/left handed microstrip leaky-wave antenna," *IEEE Microw. Wireless Compon. Lett.*, vol. 14, no. 6, pp. 277–279, Jun. 2004.
- [18] A. H. Panaretos and D. H. Werner, "Leaky-wave antennas based on capacitively tuned modulated reactance surfaces," *IEEE Antennas Wireless Propag. Lett.*, vol. 15, pp. 678–681, Aug. 2015.
- [19] A. A. Oliner and A. Hessel, "Guided waves on sinusoidally-modulated reactance surfaces," *IRE Trans. Antennas Propag.*, vol. 7, no. 5, pp. 201–208, Dec. 1959.
- [20] B. H. Fong, J. S. Colburn, J. J. Ottusch, J. L. Visher, and D. F. Sievenpiper, "Scalar and tensor holographic artificial impedance surfaces," *IEEE Trans. Antennas Propag.*, vol. 58, no. 10, pp. 3212–3221, Oct. 2010.
- [21] B. G. Cai, Y. B. Li, H. F. Ma, W. X. Jiang, Q. Cheng, and T. J. Cui, "Leaky-wave radiations by modulating surface impedance on subwavelength corrugated metal structures," *Sci. Rep.*, vol. 6, Apr. 2016, Art. no. 23974.
- [22] X. Zhang *et al.*, "Loss analysis and engineering of spoof surface plasmons based on circuit topology," *IEEE Antennas Wireless Propag. Lett.*, vol. 16, pp. 3204–3207, Nov. 2017.
- [23] G. Lovat, P. Burghignoli, and D. R. Jackson, "Fundamental properties and optimization of broadside radiation from uniform leaky-wave antennas," *IEEE Trans. Antennas Propag.*, vol. 54, no. 5, pp. 1442–1452, May 2006.
- [24] S. Paulotto, P. Baccarelli, F. Frezza, and D. R. Jackson, "A novel technique for open-stopband suppression in 1-D periodic printed leaky-wave antennas," *IEEE Trans. Antennas Propag.*, vol. 57, no. 7, pp. 1894–1906, Jul. 2009.
- [25] M. Guglielmi and D. R. Jackson, "Broadside radiation from periodic leaky-wave antennas," *IEEE Trans. Antennas Propag.*, vol. 41, no. 1, pp. 31–37, Jan. 1993.



**Meng Wang** received the B.S. degree from the Nanjing University of Science and Technology, Nanjing, China, in 2015. He is currently pursuing the Ph.D. degree with Southeast University, Nanjing, China.

His current research interests include leaky-wave antennas and spoof surface plasmon polaritons.

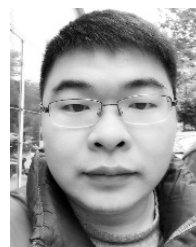
Mr. Wang was a recipient of the Best Student Paper Award at the 2018 International Conference on Microwave and Millimeter Wave Technology.



**Hui Feng Ma** received the B.S. degree in electronic engineering from the Nanjing University of Science and Technology, Nanjing, China, in 2004, and the Ph.D. degree from the State Key Laboratory of Millimeter Waves, Southeast University, Nanjing, China, in 2010.

In 2010, he joined the School of Information Science and Engineering, Southeast University, Dhaka, Bangladesh, and was promoted to Associate Professor in 2011 and Full Professor in 2015. His current research interests include metamaterial antennas, spoof surface plasmon polaritons, and other novel metamaterial functional devices including theoretical design and experimental realization.

Dr. Ma was a recipient of the Second Prize of National Award for Natural Science, China, in 2014, and the First Prize of Natural Science from the Ministry of Education, China, in 2011. His research of 3-D ground carpet cloak realized by using metamaterials has been selected as one of the "10 Breakthroughs of Chinese Science in 2010."



**Hao Chi Zhang** (S'15) received the B.E. degree in electrical engineering from the University of Electronic Science and Technology of China, Chengdu, China, in 2013. He is currently pursuing the Ph.D. degree in electromagnetic and microwave technology with Southeast University, Nanjing, China.

He is currently a Project Officer with the School of Electrical and Electronic Engineering, Nanyang Technological University, Singapore. He has authored over 40 international refereed journal papers, in highly ranked journals, including the *Laser and Photonics Review*, the *ACS Photonics*, the *IEEE TRANSACTIONS ON ANTENNA AND PROPAGATION*, and the *Applied Physics Letters*. His current research interests include microwave and millimeter-wave circuits and antennas technology, surface plasmon, and metamaterials.



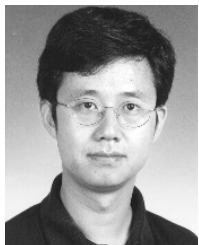
**Wen Xuan Tang** (S'10–M'13) received the B.Sc. degree in electronic engineering and the M.Sc. degree in electromagnetic field and microwave technology from Southeast University, Nanjing, China, in 2006 and 2009, respectively, and the Ph.D. degree in electromagnetics from Queen Mary University of London, London, U.K., in 2012.

In 2012, she joined the School of Information Science and Engineering, Southeast University, China, as a Lecturer, and became an Associate Professor in 2017. Her current research interests include metamaterials and their applications, and microwave devices and antennas. She has co-authored an edited book on metamaterials, two book chapters, and over 30 technical articles in highly ranked journals, including the *IEEE TRANSACTIONS ON ANTENNA AND PROPAGATION*, the *New Journal of Physics*, the *Optics Express*, the *Applied Physics Letters*, and the *Light Science and Applications*.



**Xuan Ru Zhang** received the Ph.D. degree in physics from the University of Science and Technology of China, Hefei, China, in 2014.

She was an Engineer with the 38th Institute of China Electronics Technology Group Corporation, Hefei, from 2014 to 2016. She is currently a Post-Doctoral Researcher with the State Key Laboratory of Millimeter Waves, Southeast University, Nanjing, China. Her current research interests include plasmonics, metamaterials, and optoelectronic devices.



**Tie Jun Cui** (M'98–SM'00–F'15) received the B.Sc., M.Sc., and Ph.D. degrees in electrical engineering from Xidian University, Xi'an, China, in 1987, 1990, and 1993, respectively.

In 1993, he joined the Department of Electromagnetic Engineering, Xidian University, and was promoted to an Associate Professor in 1993. From 1995 to 1997, he was a Research Fellow with the Institut für Hochfrequenztechnik und Elektronik, University of Karlsruhe, Karlsruhe, Germany. In 1997, he joined the Center for Computational Electromagnetics, Department of Electrical and Computer Engineering, University of Illinois at Urbana-Champaign, Champaign, IL, USA, first as a Postdoctoral Research Associate and then a Research Scientist. In 2001, he became a Cheung-Kong Professor with the Department of Radio Engineering, Southeast University, Nanjing, China. From 2013, he has been a Representative of People's Congress of China. He is the first author of the books *Metamaterials—Theory, Design, and Applications* (Springer, Nov. 2009) and *Metamaterials: Beyond Crystals, Noncrystals, and Quasicrystals* (CRC Press, Mar. 2016). He has authored or coauthored over 400 peer-reviewed journal papers in *Science*, *PNAS*, *Nature Communications*, *Physical Review Letters*, *Advanced Materials*, and IEEE Transactions. His current research interests include metamaterials, computational electromagnetic, wireless power transfer, and millimeter-wave technologies, which have been cited by more than 18 700 times (*h*-factor 70).

Dr. Cui was awarded a Research Fellowship from the Alexander von Humboldt Foundation, Bonn, Germany, in 1995, received a Young Scientist Award from the International Union of Radio Science in 1999, was awarded

a Cheung Kong Professor under the Cheung Kong Scholar Program by the Ministry of Education, China, in 2001, received the National Science Foundation of China for Distinguished Young Scholars in 2002, received Special Government Allowance awarded by the Department of State, China, in 2008, received the Award of Science and Technology Progress from Shaanxi Province Government in 2009, received the May 1st Labour Medal from Jiangsu Province Government in 2010, received the First Prize of Natural Science from the Ministry of Education, China, in 2011, and received the Second Prize of National Natural Science, China, in 2014. His research has been selected as one of the “Optics in 2016” by Optics and Photonics News Magazine (OSA), “10 Breakthroughs of China Optics in 2016,” “10 Breakthroughs of China Science in 2010,” “Best of 2010” in the *New Journal of Physics*, the Research Highlights in *Europhysics News*, the *Journal of Physics D: Applied Physics*, the *Applied Physics Letters*, and the *Nature China*. His work has been reported by *Nature News*, *Science*, *MIT Technology Review*, *Scientific American*, and *New Scientists*. He is an active reviewer for *Science*, *Nature Materials*, *Nature Photonics*, *Nature Physics*, *Nature Communications*, *Physical Review Letters*, *Advanced Materials*, and a series of IEEE Transactions. He was an Associate Editor of the IEEE TRANSACTIONS ON GEOSCIENCE AND REMOTE SENSING and a Guest Editor of the *Science China Information Sciences*. He served as an Editorial Staff for *IEEE Antennas and Propagation Magazine* and is in the editorial boards of the *Progress in Electromagnetic Research* and the *Journal of Electromagnetic Waves and Applications*. He served as a General Co-Chair for the International Workshops on Metamaterials (META'2008, META'2012), a TPC Co-Chair for the Asian Pacific Microwave Conference (APMC'2005) and the Progress in Electromagnetic Research Symposium (PIERS'2004). According to ELSEVIER, he is one of the most cited Chinese researchers.